NJC

PAPER

Cite this: *New J. Chem.*, 2019, **43**, 4531

Sensitive colorimetric detection for lysozyme based on the capture of a fixed thiol-aptamer on gold nanoparticles†

Yuanyang Xie, ‡[ab] Yu Huang, ‡*[a] Dongyun Tang,[a] Hongliang Cui,[b] Lizhu Yang,*[c] Haiyan Cao*[d] and Wen Yun[e]

Received 2nd January 2019,
Accepted 14th February 2019

DOI: 10.1039/c9nj00016j

rsc.li/njc

In this work, a novel simple and sensitive detection method for lysozyme based on the surface plasmon resonance of gold nanoparticles has been developed. The lysozyme aptamer constantly immobilized on the surface of gold nanoparticles *via* a thiol functional group is the recognition element of lysozyme and a stabilizer of this system. The presence of lysozyme leads to the red-shift of the resonance wavelength of gold nanoparticles in accordance with its concentration. Two factors lead to the red spectral shift of gold nanoparticles, which are the increase of the refractive index in the environment surrounding the gold nanoparticles and the aggregation of gold nanoparticles. A critical point is distinguished from the spectral shift as a function of lysozyme concentration, where the dominant power influencing the red-shift is transferred from the first one to the second one with the increase of lysozyme concentration. The limit of detection for lysozyme in this study is 0.054 nM, with a linear calibration ranging from 0.347 nM to 2.431 nM under the optimal usage conditions of 0.1250 nM thiol-aptamer functionalized gold nanoparticles. Therefore, this thiol-aptamer functionalized gold nanoparticle method provides a selective detection strategy for lysozyme and generates a great promising application.

Introduction

Lysozyme is an important defensive molecule of the innate immune system, which plays a significant role in mediating protection against microbial invasion.[1] It is commonly present in various body fluids and is considered as the body's own antibiotic.[2] In the past decades, lysozyme was found to be an indicator of many diseases, such as tuberculosis, bronchopulmonary dysplasia in newborns and rheumatoid arthritis.[3,4] Therefore, the determination of lysozyme is broadly valuable for early diagnosis and prognosis of some diseases.[5]

By now, the most employed methods for lysozyme determination are lysorocket electrophoresis, turbidimetric detection and lysoplate assay, which are widely used for the determination of lysozyme but some limitations including low sensitivity and interference from other proteins still exist.[6–8] Immunoassays and enzyme-linked immunosorbent assay have been developed recently for lysozyme determination with high sensitivity and selectivity.[9] However, expensive and unstable antibodies are the most frequently utilized in these methods, which would increase the cost of the analytical method and time consuming analysis.[10] Aptamers are small single-stranded nucleic acids with outstanding affinity and specificity.[11] Compared to antibodies, aptamers have several advantages, such as chemical synthesis, ease of modification, high stability, and target versatility.[12–14]

Gold nanoparticles (GNPs) are well known for their catalytic activity and localized surface plasmon resonance, which are strongly dependent on the local environment.[15–17] Taking into account the advantages of aptamers, a number of aptamer-based analytical methods have been fabricated with a great promise for clinical application. The easy link of GNPs to aptamers enables them to be extensively applied in biomedical fields. The surrounding refractive index (RI) and aggregation/dispersion of GNPs due to the change in the local environment provide possibilities of transducing molecular interactions into detectable colorimetric signals.[18,19] Compared to tradition methods, the combination of aptamers and GNPs offers an alternative way for lysozyme recognition strategies. Generally speaking, the strategies to bind aptamers on GNPs and consequent detection

[a] *Chongqing Institute of Green and Intelligent Technology, Chinese Academy of Sciences, Chongqing, 400714, China. E-mail: huangyu@cigit.ac.cn*
[b] *University of Chinese Academy of Science, Beijing, 100049, China*
[c] *School of Pharmaceutical Sciences, Wenzhou Medical University, Wenzhou, Zhejiang, 325035, China. E-mail: yanglz3000@aliyun.com*
[d] *School of Chemistry and Chemical Engineering, Yangtze Normal University, Chongqing, 408100, China. E-mail: 513923170@qq.com*
[e] *Chongqing Key Laboratory of Catalysis and Functional Organic Molecules, College of Environment and Resources, Chongqing Technology and Business University, Chongqing, 400067, China*

† Electronic supplementary information (ESI) available. See DOI: 10.1039/c9nj00016j

‡ These authors contributed equally to this work.

are classified into two categories by the pathway of aptamers immobilized on GNPs. The first category presented in most previous studies is that the binding of aptamers on GNPs is based on the unmodified aptamer.[6,20–23] The adsorption of aptamers on the surface of GNPs is *via* van der Waals forces and electrostatic binding forces between the bases of aptamers and GNPs. The presence of lysozyme would trigger the release of aptamers from GNPs. Then, GNPs without protection provided by aptamers would aggregate and initiate the change in signals. However, the probes are generally prepared by mixing the unmodified aptamers and gold nanoparticles just before the initiation of the detection. On the other hand, the second category is that the immobilization of aptamers on the surface of GNPs is established on the special groups of functionalized aptamers. The functionalized aptamers are constantly immobilized on the surface of GNPs during the detection process, in which *in situ* detection is achievable. Tohidi *et al.*[7] immobilized lysozyme aptamers on the surface of gold nanorods *via* Au–thiol bonds. The normal detectable 20 nM level of lysozyme of this nanoprobe in an ambient environment was improved by heat induced morphological modification of gold nanorods.

In this paper, according to the second category, we developed a simple, low cost and highly efficient aptamer based on the *in situ* lysozyme detection colorimetric method. Being different from a previous strategy,[6] the lysozyme aptamers constantly linked to the surface of GNPs are functionalized by Au–thiol bonds. According to the research of Pei *et al.*,[24] it can dramatically enhance their stability even if the surrounding environment is at a high salt level. Thus, this method implies that the probe can be stored for a long time after preparation. The LOD of lysozyme at 0.054 nM has been achieved in a normal thermal environment. The mechanism of this lysozyme detection method has been systematically investigated. The change in the local refractive index and the aggregation of GNPs due to the presence of lysozyme lead to the shift of plasmon resonance of GNPs. This understanding of the lysozyme detection method originating from the monitoring of lysozyme thiol-aptamer functionalized GNPs can promote the designation of the lysozyme determination method and expand its further application in the future.

Experimental section

Materials

Lysozyme from chicken egg white, pepsin from porcine gastric mucosa, choline oxidase (ChOx) from *Alcaligenes*, glucose oxidase from *Aspergillus niger* (GOx), and hydrogen tetrachloroaurate(III) trihydrate ($HAuCl_4{\cdot}3H_2O$) were obtained from Sigma. Bovine serum albumin (BSA) and human serum albumin (HSA) were purchased from Shanghai Biological Technology Development Co., Ltd. Trisodium citrate anhydrous was procured from Alfa Aesar. Tris(2-carboxyethyl)phosphine hydrochloride (TCEP), acetate, and L-lysine (Lys) were purchased from Aladdin. The 5′-thiol-modified DNA aptamer of lysozyme (5′HS-ATC AGG GCT AAA GAG TGC AGA GTT ACT TAG-3′)[25] was obtained from Shanghai Sangon Biotech Co., Ltd. Sodium acetate trihydrate and tris(hydroxymethyl)aminomethane (Tris) were purchased from BBI Life Sciences. HCl, NaH_2PO_4, Na_2HPO_4, and NaCl were procured from Chongqing Chuandong Chemical (Group) Co., Ltd. All reagents were of at least analytical grade. The ultrapure water used throughout the work had a resistivity higher than 18.00 MΩ cm^{-1}.

Apparatus

A custom-made absorption spectroscope shown in Fig. S1 (ESI†) was utilized to record the spectra. A tungsten halogen lamp (HL-2000-HP, Ocean Optics) is used as a light source to illuminate the sample, which is contained in a 1 cm path-length quartz cuvette in the dark. The absorbance from the sample was recorded using a spectrometer (HR4000, Ocean Optics) and analysed by programs written in C++ and Matlab. TEM images were obtained using a Zeiss LIBRA 200FEG TEM. The samples were lyophilized on copper coated grids. The size of the particles was detected by dynamic light scattering (DLS) and zeta potentials were obtained by Malvern Zetasizer Nano ZS.

Preparation of GNPs

The GNPs of about 12 nm in diameter were synthesized *via* previously described sodium citrate reduction methods.[26] Briefly, spherical GNPs were prepared by adding 15 mL of 1% trisodium citrate solution to 100 mL of boiling 1 mM $HAuCl_4$ solution under vigorously stirring and continuing heating for 15 min. Then, the solution was cooled down to room temperature filtered by a 0.22 mm PES Syringe Filters and stored at 4 °C before functionalization.

Probe fabrication

Thiol-aptamer functionalized gold nanoparticles (HS-Aptamer@GNPs) were prepared with a method reported in the literature.[27] Firstly, 3 μL of 1 mM 5′-thiol aptamer were activated by mixing with 0.5 μL of 10 mM freshly prepared TCEP and 0.5 μL of 500 mM acetate buffer (pH 5.2) at room temperature for 1 h. Then this solvent was added to 3 mL prepared GNP solution. The mixture was incubated in a drawer at room temperature for at least 16 h. Next, in order to maximize the amount of aptamer loaded on the surface of GNPs, 30 μL of 500 mM Tris acetate buffer (pH 8.2) and 300 μL of 1 M NaCl were added dropwise and stored in a drawer at room temperature for at least 24 h.

Purification of HS-aptamer@GNPs

3 ml of HS-aptamer@GNPs were centrifuged at 16 200*g* at room temperature for 15 min and the precipitate was diluted by ultrapure water to be 3 mL. The procedures were repeated once again to remove freely abundant aptamers and ions. The concentration of HS-aptamer@GNPs was recorded according to the concentration of GNPs calculated by the extinction coefficient at 520 nm as GNPs.[27] The purified HS-aptamer@GNPs were stored at 4 °C for further use.

Target detection with HS-aptamer@GNPs

The procedure for lysozyme detection was carried out as follows: 50 μL of HS-aptamer@GNPs, 300 μL of 1 M NaCl, 100 μL of 0.2 M acetate buffer (pH 4.0) and 1550 μL of different concentrations of

lysozyme were added to a 2 mL micro centrifuge tube, and the mixture was shaken thoroughly and incubated at room temperature for 1 h. The concentration of HS-aptamer@GNPs was 0.1250 nM after this preparation. The absorption spectrum was recorded from 400 nm to 800 nm, and the shift of resonance wavelength was used for quantitative analysis. All the data were collected from at least three independent measurements. The sensitivity of detection was tested by monitoring different parameters, including HS-aptamer@GNP concentration, ionic strength and pH values. The specificity of the probe was tested by control proteins.

Results and discussion

Characterization of HS-aptamer@GNPs

Fig. 1A depicts the absorption spectra of GNPs and HS-aptamer@GNPs and the morphology of HS-aptamer@GNPs, respectively. Prior to nanoprobe fabrication, the citrate-protected GNPs of about 12 nm in diameter exhibit plasmon resonance at about 518 nm. The binding of aptamers on GNPs replaces the citrate on the surface of GNPs with thiol-functional aptamers, resulting in an increase in the refractive index of the local environment surrounding GNPs. The shift of resonance wavelength from 518 nm to 524 nm confirms the successful immobilization of aptamers on the surface of GNPs.[28] According to the research of Li *et al.*,[29] the addition of targets would decrease the degree of aggregation triggered by the addition of $MgCl_2$. It is a reverse trend compared with the GNP probe functionalized by unmodified aptamers. Furthermore, Fig. 1B shows after being triggered by $MgCl_2$ the shift of the probe in the presence of lysozyme is less than the shift in the absence of lysozyme. It also proves that the HS-aptamer was functionalized completely on the surface of GNPs.

The comparison of the zeta potentials of GNPs and HS-aptamer@GNPs dispersing in ultrapure water was carried out as shown in Fig. S2 (ESI†). The decrease in zeta potential from −30.92 mV to −41.02 mV is attributed to the presence of negative charge of the phosphate backbone, which is another evidence for the successful immobilization of aptamers on the surface of GNPs. Furthermore, the more negative zeta potential exhibited by the HS-aptamer@GNPs indicates that the binding force between aptamers and GNPs is Au–thiol bonds, rather than the weak electrostatic adsorption. The absolute value of zeta potential of more than 20 mV is of benefit to control the distance between nanoparticles in solvent, which is useful to extend the storage of solution.[25] The spectra of HS-aptamer@GNPs were continuously recorded for more than 6 months and their mere shift proves the stability of the solution (the absorption spectra are shown in Fig. S3, ESI†).

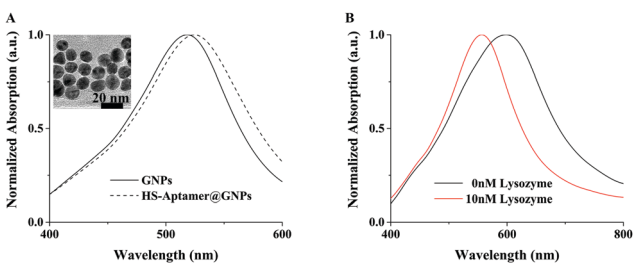

Fig. 1 (A) Normalized absorption spectra of GNPs (solid line) and HS-aptamer@GNPs (dashed line) (inset: size and morphology of HS-aptamer@GNPs with a diameter of ~12 nm) (scale bar corresponds to 20 nm). (B) Normalized absorption spectra of HS-aptamer@GNPs with 0 nM lysozyme (black line) and 10 nM lysozyme (red line) after incubating $MgCl_2$.

Effect of pH

pH is a significant parameter in the water environment. In order to select the optimal pH suitable for the detection, acetate buffer and phosphate buffer with a concentration of 0.01 M in the final detection system were used to adjust the pH of solvent with 0.05 M NaCl, 0.1250 nM HS-aptamer@GNPs, and 3.472 nM lysozyme. The spectral shift of GNPs due to the different pH environment is shown in Fig. 2. A comparable spectral shift generated by the environment with different pH values indicates that the pH is an important control factor in this test. The spectral shift is small at pH higher than 7.0. Additionally, as shown in Fig. S4 (ESI†), by increasing the concentration of lysozyme from 3.472 nM to 1.042 μM in a buffer with pH 5.0, the spectral shift of HS-aptamer@GNPs is always about 30 nm. However, the spectral shift is improved dramatically from nearly 3 nm to 28 nm with the increase of lysozyme concentration in buffer with pH 7.0. At a certain concentration of HS-aptamer@GNPs, the addition of more lysozyme can induce larger spectral shift meaning that the capture activity of aptamers immobilized on the GNPs is influenced by the value of pH. The decrease in the degree of capture activity of aptamers in a higher pH environment may contribute to this negligible spectral shift under higher pH conditions.

On the other hand, the activity of aptamers is improved significantly with the decrease in pH. As a result, more and more lysozyme can be captured, which increases the spectral shift of GNPs until a plateau is approached at a pH of about 3.0. According to the research of Yuan *et al.*,[30] the zwitterionic ligand-modified GNPs are aggregated by the mediation of

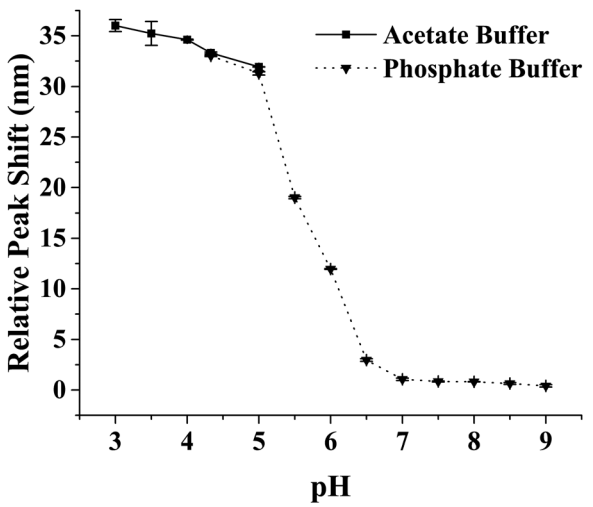

Fig. 2 The spectral shift of 0.1250 nM HS-aptamer@GNPs due to the presence of 3.472 nM lysozyme in different pH environments with 0.05 M NaCl.

hydrogen bonds between protonated sulfonic acid groups of zwitterionic ligands on one GNP and the neighbouring groups on another nanoparticle, represented as S–O–H···O═S. Similarly, an environment with lower pH is beneficial for the phosphate groups of aptamers to protonate and promote their connection with neighbouring phosphate groups, which formed as P–O–H···O═P. Additionally, the protonation from phosphate groups can decrease the zeta potential and reduce the repulsion between GNPs to promote aggregation.[31] Thus, the promotion of protonation from phosphate groups to strengthen the attraction between GNPs is the reason for the signal enhancement with a decrease in pH. However, the pH of the environment lower than 4.0 weakens the stability of GNPs reflected by the increase of the standard deviation.

Hence, a suitable pH value is able to detect the protonation of phosphate groups and enhance the degree of aggregation of GNPs. To balance the high sensitivity and stability, a pH of 4.0 is chosen in the following experiments.

Effect of ionic strength

Ionic strength is another essential factor to influence the experiment. The increase in ionic strength would weaken the interparticle repulsive force and affect the degree of aggregation of GNPs.[32] Therefore, it is necessary to monitor the effect of ionic strength to optimize this detection. NaCl was chosen to control ionic strength with different concentrations and the spectral shift of HS-aptamer@GNPs with and without lysozyme in different ionic strengths is shown in Fig. 3.

In 0.01 M acetate buffer of pH 4.0, the resonance wavelength of HS-aptamer@GNPs without lysozyme exhibits little change until the NaCl concentration became higher than 0.25 M, which indicates that the aggregation of GNPs is initialized from this NaCl concentration level. Higher concentrations of NaCl reduce the thickness of the electrostatic double layer of GNPs, which decreases the absolute value of zeta potential and promotes the aggregation of HS-aptamer@GNPs.[33,34] By contrast, the addition of 3.472 nM lysozyme breaks the charge screening of HS-aptamer@GNPs and enables their aggregation even when the concentration of NaCl is extremely low. The higher the concentration of NaCl is, the longer the resonance wavelength shift will be. However, it is noted that there is a zig-zag tendency of resonance wavelength as a function of NaCl concentrations when the NaCl concentration is in the range between 0.15 M and 0.45 M. Qiao *et al.* reported that β-glucuronidase can be tightly captured within 0.15 mM NaCl by aptamers and the partial target will be washed off when the concentration of NaCl is 0.33 M, which reveals that the ability of aptamers to capture β-glucuronidase can decrease with increasing ionic strength when the ionic strength approaches a specific density.[35] Therefore, the capability of aptamers is weakened in a specific range of NaCl concentrations. Then, 0.15 M NaCl is used in the following experiment for high sensibility.

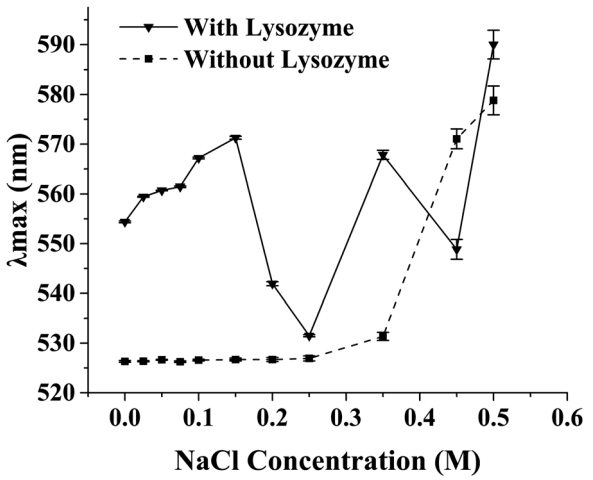

Fig. 3 The resonance wavelength of 0.1250 nM HS-aptamer@GNPs without and with the addition of 3.472 nM lysozyme at different NaCl concentrations. The environmental conditions are pH 4.0 and 0.01 M acetate buffer.

Effect of HS-aptamer@GNP concentration and the detection of lysozyme

Under the aforementioned optimized conditions, which is 0.01 M acetate buffer at pH 4.0 and 0.15 M NaCl, the performance of 0.0625 nM, 0.1250 nM and 0.2500 nM of HS-aptamer@GNPs was investigated by the addition of different concentrations of lysozyme. The spectral responses of HS-aptamer@GNPs with different concentrations in the presence of lysozyme are shown in Fig. 4A–C. Higher concentrations of lysozyme in the range of detection shift the resonance wavelength further to the red region.

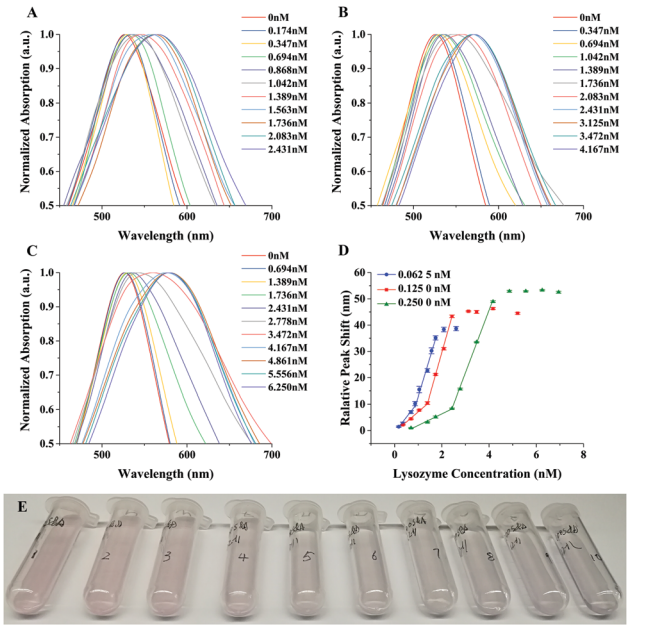

Fig. 4 The detection of lysozyme with 0.01 M pH 4.0 acetate buffer and 0.15 M NaCl. The normalized spectral response to different lysozyme concentrations with HS-aptamer@GNPs of (A) 0.0625 nM, (B) 0.1250 nM, and (C) 0.2500 nM (D). The resonance wavelength shift as a function of lysozyme concentrations of HS-aptamer@GNPs with 0.0625 nM (blue), 0.1250 nM (red) and 0.2500 nM (green) HS-aptamer@GNPs. (E) Photographs of 0.2500 nM HS-aptamer@GNPs corresponding to the green line shown in (D).

The change in colour due to the presence of lysozyme can be seen by the naked eye as illustrated in Fig. 4E. It is interesting to note that the spectral responses are stronger for lower concentrations of HS-aptamer@GNPs when the lysozyme concentration is lower than a specific level. Taking the performance of 0.0625 nM HS-aptamer@GNPs shown in Fig. 4D as an example, its spectral shift is the highest when the lysozyme concentration is lower than approximately 1.8 nM. Furthermore, an increase in lysozyme concentration hardly shifts the resonance wavelength of 0.0625 nM HS-aptamer@GNPs anymore. In order to detect higher concentrations of lysozyme, it is better to use a high concentration of HS-aptamer@GNPs as the probe.

Furthermore, a critical point, which divides the spectral response of HS-aptamer@GNPs to lysozyme into two parts, apparently presents the spectral shift as a function of lysozyme concentrations (Fig. 4D). Comparing the performance of these three kinds of HS-aptamer@GNP concentrations, HS-aptamer@GNPs with a lower concentration has better sensitivity before this critical point but with poorer limit of detection as shown in Table S1 (ESI†). However, after this critical point, the tendency is reversed that is higher concentration HS-aptamer@GNPs possessed a broader range of detection limits. Taking the sensitivity and limit of detection into consideration, 0.1250 nM HS-aptamer@GNPs exhibit a good performance in the detection of lysozyme. The linear range is 0.347 nM to 2.431 nM and the LOD (3σ) for lysozyme is 0.054 nM. Compared with the existing methods (Table S2, ESI†), the method demonstrated superiority in detection sensitivity.

Saliva was chosen as a real sample to test this method. Two kinds of saliva were diluted 12 000 times to match the linear range of this method and their pH was adjusted to the optimal parameter. To further confirm the suitability and repeatability of this method, other 4 spiked samples were prepared and each sample was detected three times. The results are shown in Table 1. The 94.0–105.9% recoveries confirm that this method has the potential application for real samples. Then, the concentration of lysozyme in the original two kinds of saliva was detected by using the national standard of the People's Republic of China: GB/T 25789-2010. After dividing into 12 000 times, the concentration of lysozyme was found to be 0.445 ± 0.011 nM and 0.722 ± 0.070 nM in saliva_a and saliva_b, respectively. This concentration detected by the standard method is in accordance with that detected by our method. Thus, our method further proves that it has potential application.

Table 1 Determination of lysozyme from salivary samples

Sample no.[a]	Add (nM)	Found[b] (nM)	Recovery (%)
a1	0	0.438 ± 0.079	—
a2	0.5	0.962 ± 0.053	104.8
a3	1	1.497 ± 0.087	105.9
b1	0	0.712 ± 0.098	—
b2	0.5	1.201 ± 0.044	97.8
b3	1	1.652 ± 0.121	94.0

[a] The salivary sample was diluted 12 000 times. [b] The average and standard deviation of three detections with this method (mean ± SD).

Specificity of target detection

The specificity of the detection was investigated by using different proteins, including pepsin, glucose oxidase (GOx), choline oxidase (ChOx), bovine serum albumin (BSA), human serum albumin (HSA) and L-lysine (Lys), at pH 4.0, 0.15 M NaCl and 0.1250 nM HS-aptamer@GNPs. The isoelectric point (pI) value of pepsin is 1.0 and lower than the detecting pH (4.0).[36] However, the pI values of GOx, ChOx, BSA, HAS and Lys are 5.0, 4.5, 4.9, 4.7 and 9.5 respectively.[37–41] Their pI values are similar to that of lysozyme (pI: 10.8) which is higher than 4.0.[36] Fig. 5 illustrates that only lysozyme can cause an apparent spectral shift, although the concentrations of control proteins are 300 times that of lysozyme, revealing the high specificity this proposed aptamer-based method has. The mixture contains all the foreign proteins excluding pepsin to avoid the degradation of lysozyme with the same concentration of lysozyme. The response of this proposed method to the mixture further implies that the other foreign proteins have almost little impact on the response in the presence of lysozyme and this method has specificity for lysozyme detection.

Mechanism of HS-aptamer@GNP detection

It is worth noting that the relative spectral shifts of HS-aptamer@GNPs from bare to the presence of lysozyme at critical points are approximately 10 nm (Fig. 4D). This is comparable to the results investigated by Truong *et al.*[42] and Park *et al.*,[43] who generated nearly 14 nm and 10 nm spectral shifts by monitoring GNPs respectively. The difference between this proposed method and their method is that they immobilized GNPs on a glass slide while the GNPs is free in solvent in this proposed method. The aggregation of GNPs would not be present in their case because the nanostructures were immobilized on a glass substrate. Considering the spectral shift as a function of lysozyme

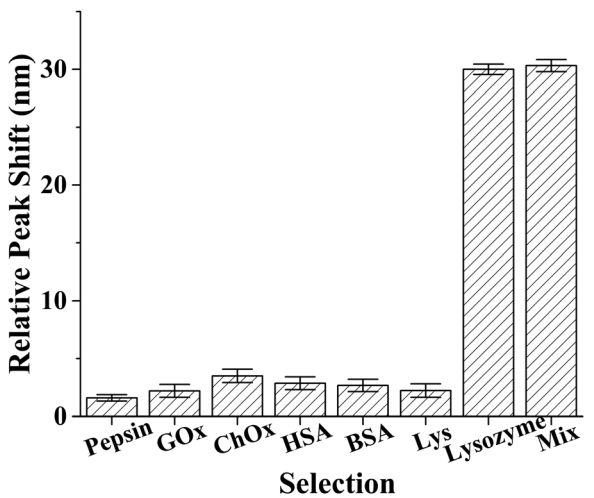

Fig. 5 The specificity test of 0.1250 nM HS-aptamer@GNP probe, with an environment of 0.01 M acetate buffer, 0.15 M NaCl and pH 4.0, for different control proteins. The concentrations of pepsin, GOx, ChOx, HAS, BSA and Lys were 600 nM and the lysozyme concentrations were 2.00 nM. The mixture had 0.2 nM GOx, 0.2 nM ChOx, 0.2 nM HSA, 0.2 nM BSA, 0.2 nM Lys and 0.2 nM lysozyme.

concentration shown in Fig. 4D, at a certain lysozyme concentration level before the critical point of each concentration of HS-aptamer@GNPs, a smaller amount of HS-aptamer@GNPs captures more lysozyme, which leads to a bigger spectral shift while this tendency is reversed after this critical point. The surface charge of HS-aptamer@GNPs is negative while the charges of GOx, ChOx, BSA and HSA are positive. The addition of these foreign proteins does not shift the spectrum of HS-aptamer@GNPs significantly, which means that electrostatic adsorption taking place between these proteins and HS-aptamer@GNPs does not strongly induce the aggregation of HS-aptamer@GNPs. Thus, a hypothesis is proposed as shown in Scheme 1, the dominant factor to determine the spectral shift is transfer from the change of the refractive index to the aggregation of GNPs at this critical point. At a lower lysozyme concentration, the change in the refractive index is a major factor to shift the spectrum of GNPs while the aggregation of GNPs gradually dominates this phenomenon when the lysozyme concentration is higher.

To further confirm this hypothesis, a comparison of the zeta potential, particle size measured by DLS and TEM photographs recorded before and after the critical point was carried out. Fig. 6 demonstrates that the absolute value of zeta potential decreases with the addition of lysozyme before the critical point. A new hybrid particle composed of negative HS-aptamer@GNPs and positive lysozyme is generated, leading to the neutralization of zeta potential.[44,45] However, after the critical point, the zeta

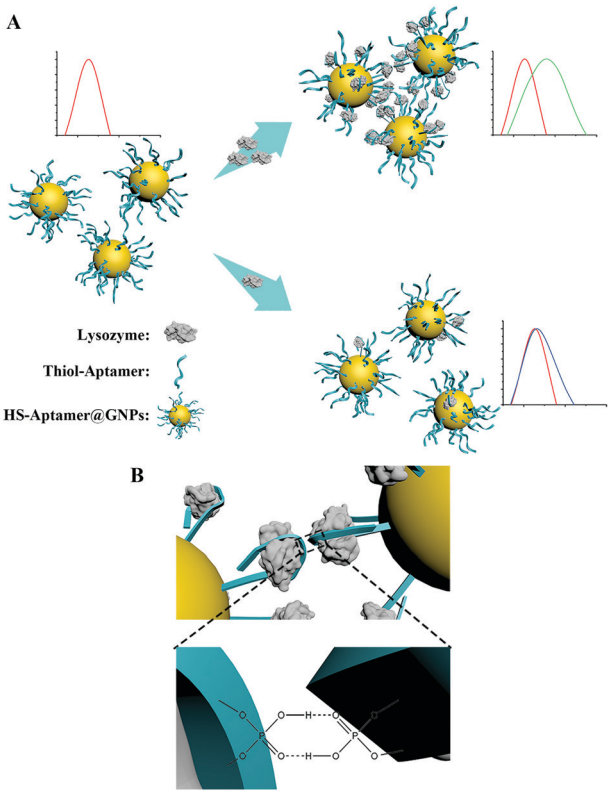

Scheme 1 (A) Respond of HS-aptamer@GNPs to the presence of lysozyme. (B) Mechanism of the aggregation of HS-aptamer@GNPs.

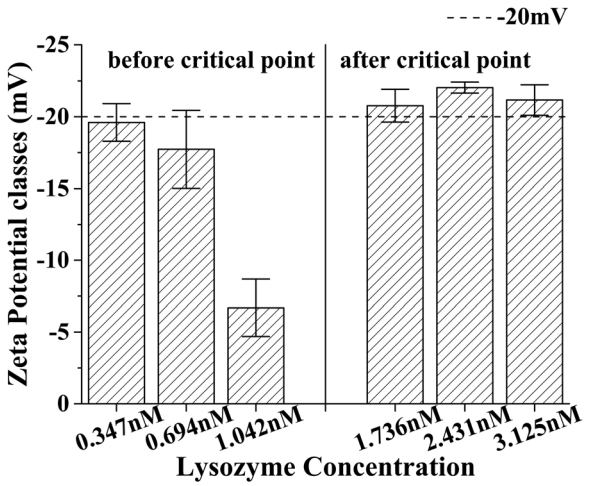

Fig. 6 Zeta potential for 0.1250 nM HS-aptamer@GNPs (in the solution of 0.15 M NaCl and 0.01 M acetate buffer, pH 4.0) with different lysozyme concentrations.

potential tends to be independent of the lysozyme concentration. The aggregation process of GNPs is regarded to be analogous to that of micelle growth. The aggregation of HS-aptamer@GNPs induced by the phosphate groups of aptamers, which have captured lysozyme, orients the captured lysozyme toward the inner space of the hybrid by the interaction of hydrogen bonds. Comparatively, the aptamer that does not capture lysozyme is located outside the hybrid. This prevents the generation of more aggregates. As shown in Fig. 7, before the critical point, the aggregates are not present in the TEM images, and the size distribution of GNPs shows a slight change with the addition of 0.694 nM lysozyme compared to the particle size distribution without the addition of lysozyme. Nevertheless, after the critical point, the particle size distribution measured by DLS shows an obvious change with the addition of 6.944 nM lysozyme compared to that

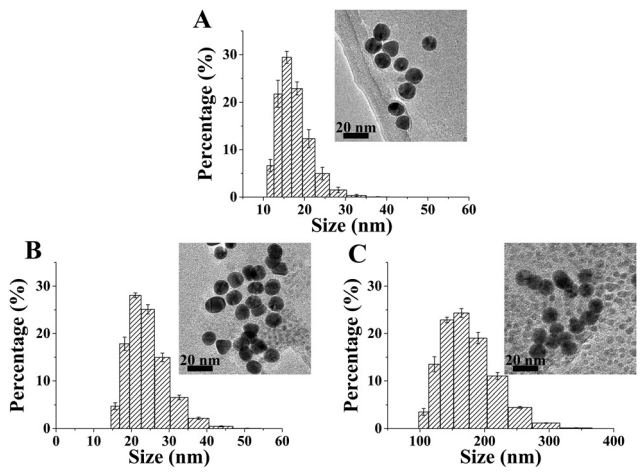

Fig. 7 TEM images and particle size distributions detected by DLS of 0.1250 nM HS-aptamer@GNPs (in the solution of 0.15 M NaCl and 0.01 M acetate buffer, pH 4.0, after 1 hour) (A) without lysozyme, (B) with 0.694 nM lysozyme (before the critical point), and (C) with 6.944 nM lysozyme (after the critical point) (scale bar corresponds to 20 nm).

without lysozyme. In one word, all the results on zeta potential, TEM images and size distribution by DLS are consistent with the hypothesis, and two factors, the refractive index of the local environment and the aggregation of GNPs, would dominate the spectral shift of GNPs induced by the presence of lysozyme at different stages.

Conclusions

A simple and ultrasensitive method for the quantitative detection of lysozyme based on the thiol-aptamer functionalized GNPs has been demonstrated. The aptamer is immobilized on the surface of GNPs *via* thiol functional groups, which enhances the stability of this probe at high salt concentrations. The capture of lysozyme by aptamers leads to the spectral shift of GNPs. Two factors influencing the spectral shift of GNPs, which are the change in the refractive index and the aggregation of GNPs, have been systematically investigated. The dominator to control the spectral shift is transferred from the change in the refractive index to the aggregation of GNPs with the increase of lysozyme concentrations. The best limit of detection for lysozyme was 0.054 nM for the utilization of 0.1250 nM HS-aptamer@GNPs in this study. This proposed method provides an alternative way for the detection of lysozyme at ultralow concentrations. Furthermore, because of the captured part based on the aptamers of lysozyme, it can be applied in a wide range of analyte detection methods by altering different kinds of aptamers.

Conflicts of interest

There are no conflicts to declare.

Acknowledgements

This work is sponsored by the National Natural Science Foundation of China (Grant No. 21707137), the Key Application and Development Program of Chongqing (No. cstc2017shmsA0159), the Natural Science Foundation of Chongqing (Grant No. cstc2018jcyjAX0718), the Research Funding Project of Yangtze Normal University (No. 2017KYQD23), the Young Scientist Research Fund of Yangtze Normal University, and the Open Research Fund Program of Key Laboratory of Reservoir Aquatic Environment of CAS.

Notes and references

1 V. A. Proctor and F. E. Cunningham, *Crit. Rev. Food Sci. Nutr.*, 1988, **26**, 359–395.
2 S. Saurabh and P. K. Sahoo, *Aquacult. Res.*, 2008, **39**, 223–239.
3 C. Serra, F. Vizoso, L. Alonso, J. C. Rodriguez, L. O. Gonzalez, M. Fernandez, M. L. Lamelas, L. M. Sanchez, J. L. Garcia-Muniz, A. Baltasar and J. Medrano, *Breast Cancer Res.*, 2002, **4**, R16.
4 S. A. Ragland and A. K. Criss, *PLoS Pathog.*, 2017, **13**, e1006512.
5 S. Wang, T. B. Ng, T. Chen, D. Lin, J. Wu, P. Rao and X. Ye, *Biochem. Biophys. Res. Commun.*, 2005, **327**, 820–827.
6 X. Wang, Y. Xu, Y. Chen, L. Li, F. Liu and N. Li, *Anal. Bioanal. Chem.*, 2011, **400**, 2085–2091.
7 T. Tohidi Moghadam and B. Ranjbar, *Talanta*, 2015, **144**, 778–787.
8 D. Ercan and A. Demirci, *Crit. Rev. Biotechnol.*, 2016, **36**, 1078–1088.
9 B. Kerkaert, F. Mestdagh and B. D. Meulenaer, *Food Chem.*, 2010, **120**, 580–584.
10 Y. S. Kim, N. H. Raston and M. B. Gu, *Biosens. Bioelectron.*, 2016, **76**, 2–19.
11 S. Gao, X. Zheng, B. Hu, M. Sun, J. Wu, B. Jiao and L. Wang, *Biosens. Bioelectron.*, 2017, **89**, 952–958.
12 M. Citartan, E.-S. Ch'ng, T. S. Rozhdestvensky and T.-H. Tang, *Microchem. J.*, 2016, **128**, 187–197.
13 N. Alizadeh, M. Y. Memar, S. R. Moaddab and H. S. Kafil, *Biomed. Pharmacother.*, 2017, **93**, 737–745.
14 L. Farzin, M. Shamsipur and S. Sheibani, *Talanta*, 2017, **174**, 619–627.
15 Y. Gu, J. Song, M. X. Li, T. T. Zhang, W. Zhao, J. J. Xu, M. Liu and H. Y. Chen, *Anal. Chem.*, 2017, **89**, 10585–10591.
16 X. Wei, Z. Chen, L. Tan, T. Lou and Y. Zhao, *Anal. Chem.*, 2017, **89**, 556–559.
17 H. Su, B. Sun, L. Chen, Z. Xu and S. Ai, *Anal. Methods*, 2012, **4**, 3981.
18 N. J. Halas, S. Lal, W. S. Chang, S. Link and P. Nordlander, *Chem. Rev.*, 2011, **111**, 3913–3961.
19 F. Wang, S. Liu, M. Lin, X. Chen, S. Lin, X. Du, H. Li, H. Ye, B. Qiu, Z. Lin, L. Guo and G. Chen, *Biosens. Bioelectron.*, 2015, **68**, 475–480.
20 L. Chen, N. Xia, T. Li, Y. Bai and X. Chen, *Microchim. Acta*, 2016, **183**, 2917–2923.
21 X. Yao, X. Ma, C. Ding and L. Jia, *Microchim. Acta*, 2016, **183**, 2353–2359.
22 P. Gu, X. Liu, Y. Tian, L. Zhang, Y. Huang, S. Su, X. Feng, Q. Fan and W. Huang, *Sens. Actuators, B*, 2017, **246**, 78–84.
23 P. Wang, Y. Wan, A. Ali, S. Deng, Y. Su, C. Fan and S. Yang, *Sci. China: Chem.*, 2015, **59**, 237–242.
24 H. Pei, F. Li, Y. Wan, M. Wei, H. Liu, Y. Su, N. Chen, Q. Huang and C. Fan, *J. Am. Chem. Soc.*, 2012, **134**, 11876–11879.
25 S. Liu, W. Na, S. Pang, F. Shi and X. Su, *Analyst*, 2014, **139**, 3048–3054.
26 A. Shiohara, J. Langer, L. Polavarapu and L. M. Liz-Marzan, *Nanoscale*, 2014, **6**, 9817–9823.
27 J. Liu and Y. Lu, *Nat. Protoc.*, 2006, **1**, 246–252.
28 L. Guo, Y. Xu, A. R. Ferhan, G. Chen and D. H. Kim, *J. Am. Chem. Soc.*, 2013, **135**, 12338–12345.
29 W. Zhao, W. Chiuman, J. C. Lam, S. A. McManus, W. Chen, Y. Cui, R. Pelton, M. A. Brook and Y. Li, *J. Am. Chem. Soc.*, 2008, **130**, 3610–3618.
30 S. Yuan, X. Heng, Q. Zhang and J. Hu, *Colloids Surf., A*, 2016, **506**, 6–12.
31 M. Doukkali, R. B. Patel, V. Stepanov and H. Hadim, *Propellants, Explos., Pyrotech.*, 2017, **42**, 1066–1071.
32 K. Sun, N. Xia, L. J. Zhao, K. Liu, W. J. Hou and L. Liu, *Sens. Actuators, B*, 2017, **245**, 87–94.
33 R. Pastor, J. I. Calvo, P. Prádanos and A. Hernández, *J. Membr. Sci.*, 1997, **137**, 109–119.

34 B. J. Kirby and E. F. Hasselbrink, Jr., *Electrophoresis*, 2004, **25**, 187–202.
35 L. Qiao, B. Lv, X. Feng and C. Li, *J. Biotechnol.*, 2015, **203**, 68–76.
36 G. Li, T. Li, Y. Li, L. An, W. Li and Z. Zhang, *Colloids Surf., A*, 2017, **531**, 173–181.
37 M. Kujda, Z. Adamczyk and M. Ciesla, *Colloids Surf., B*, 2016, **148**, 229–237.
38 C. V. D. Santos Jr, M. S. Sader, G. C. Goncalves, G. Weissmuller and R. A. Simao, *Colloids Surf., B*, 2018, **167**, 441–447.
39 M. Hes, A. Gliszczynska-Swiglo and A. Gramza-Michalowska, *Acta Sci. Pol., Technol. Aliment.*, 2017, **16**, 53–67.
40 F. Zhou, X. Pu, D. Luo, G. Yin, K. Zhuang, X. Liao, Z. Huang, X. Chen and Y. Yao, *J. Biosci. Bioeng.*, 2015, **120**, 9–16.
41 S. Ikuta, S. Imamura, H. Misaki and Y. Horiuti, *J. Biochem.*, 1977, **82**, 1741–1749.
42 P. L. Truong, S. P. Choi and S. J. Sim, *Small*, 2013, **9**, 3485–3492.
43 J. H. Park, J. Y. Byun, H. Jang, D. Hong and M. G. Kim, *Biosens. Bioelectron.*, 2017, **97**, 292–298.
44 P. Bansal, A. P. Deshpande and M. G. Basavaraj, *J. Colloid Interface Sci.*, 2017, **492**, 92–100.
45 I. Ostolska and M. Wiśniewska, *J. Mol. Liq.*, 2017, **241**, 952–958.

